Mathematical Biosciences 277 (2016) 77–88

Contents lists available at ScienceDirect

Mathematical Biosciences

journal homepage: www.elsevier.com/locate/mbs

Atomic force microscopy indentation and inverse analysis for non-linear viscoelastic identification of breast cancer cells

Nhung Nguyen[a,b], Yue Shao[a], Alan Wineman[a], Jianping Fu[a], Anthony Waas[b,*]

[a] Department of Mechanical Engineering, University of Michigan, Ann Arbor, MI 48109, United States
[b] William E. Boeing Department of Aeronautics and Astronautics, Seattle, WA 98195-2400, United States

ARTICLE INFO

Article history:
Received 3 January 2016
Revised 27 March 2016
Accepted 31 March 2016
Available online 21 April 2016

Keywords:
Non-linear viscoelastic (NLV)
Atomic force microscopy (AFM)
Breast cancer cells
Inverse analysis
Surrogate
Kriging predictor

ABSTRACT

Breast cancer cells (MCF-7 and MCF-10A) are studied through indentation with spherical borosilicate glass particles in atomic force microscopy (AFM) contact mode in fluid. Their mechanical properties are obtained by analyzing the recorded reaction force–time response. The analysis is based on comparing experimental data with predictions from finite element (FE) simulation. Here, FE modeling is employed to simulate the AFM indentation experiment which is neither a displacement nor a force controlled test. This approach is expected to overcome many underlying problems of the widely used models such as Hertz contact model due to its capability to capture the contact behaviors between the spherical indentor and the cell, account for cell geometry, and incorporate with large strain theory. In this work, a non-linear viscoelastic (NLV) model in which the viscoelastic part is described by Prony series terms is used for the constitutive model of the cells. The time-dependent material parameters are extracted through an inverse analysis with the use of a surrogate model based on a Kriging estimator. The purpose is to automatically extract the NLV properties of the cells with a more efficient process compared to the iterative inverse technique that has been mostly applied in the literature. The method also allows the use of FE modeling in the analysis of a large amount of experimental data. The NLV parameters are compared between MCF-7 and MCF-10A and MCF-10A treated and untreated with the drug Cytochalasin D to examine the possibility of using relaxation properties as biomarkers for distinguishing these types of breast cancer cells. The comparisons indicate that malignant cells (MCF-7) are softer and exhibit more relaxation than benign cells (MCF-10A). Disrupting the cytoskeleton using the drug Cytochalasin D also results in a larger amount of relaxation in the cell's response. In addition, relaxation properties indicate larger differences as compared to the elastic moduli like instantaneous shear modulus. These results may be useful for disease diagnosing purposes.

1. Introduction

The knowledge of mechanical characteristics of biological cells is essential for various applications. Such an application is the manufacture of engineered polymeric synthetic cells that can mimic and replace real cells [1]. For this purpose, it is necessary to make synthetic cells mechanically resemble real cells by matching their mechanical properties. Therefore, understanding cells' mechanical responses is beneficial in the selection of materials for the manufacture process as well as examining the effectiveness of the engineered cells. Another application is related to the study of the physiology of biological cells. As many cells' functions and processes have been known to be significantly influenced by external mechanical stimuli [2–7], the knowledge of cell mechanics might lead to better quantification of many cells' physiological mechanisms. Additionally, cell mechanics is closely linked with alterations in cytoskeletal structures, which may be associated with invasive diseases such as cancer. Therefore, such knowledge might also play an important role in formulating potential biomarkers for disease detection. For example, the difference in cell stiffness between cancerous and their corresponding normal cells have been investigated in several studies [8,9]. Initial results indicated that certain types of diseased cells might be softer and more deformable. Furthermore, changes in cell stiffness have been reported between different states of cancer. The studies in [10–13] showed that as cells transform from benign to malignant stages, the stiffness exhibits a decreasing trend. In addition to stiffness, the viscoelastic behavior of the cells has also been observed [12–15], but this still requires further investigation, especially at the large deformation range. Preliminary results suggest

* Corresponding author. Tel.: +1 2066171362.
E-mail address: awaas@aa.washington.edu, dcw@umich.edu (A. Waas).

http://dx.doi.org/10.1016/j.mbs.2016.03.015
0025-5564/

that viscoelastic characteristics may be effective indicators and biomarkers for better diagnosis and treatment of this dangerous disease, and could also aid testing the efficiency of anti-cancer drugs to combat cancer.

Currently, in order to obtain the mechanical characteristics of biological cells, techniques such as micropipette aspiration [2,16–18], atomic force microscopy [2,6], magnetic twisting cytometry [2,3,19], and optical trap [20] based testing are available. Amongst them it appears that contact of a cell with a "rigid" indentor, followed by measurement of the sample response to controlled motion of the indentor, is a common technique by which the cell properties are probed. The measured data is then interpreted by formulating and solving a corresponding boundary value problem with an assumed constitutive model for the cell material. However, this interpretation is still a challenging problem and highly dependent on the chosen model. In the case of AFM indentation test [6,11–13,21,22], the Hertz contact model [23] has been frequently used to analyze the data. Nevertheless, this model is only valid under the restrictions of many assumptions such as small strain, infinitesimal elastic deformation [23,24] which are not normally satisfied in the actual context of an AFM indentation test. In order to account for the cases where large deformation occurs, AFM indentation tests should be studied using approaches which can include the consideration of non-linear mechanics. Such an approach interprets the experimental data using the FE method to take into account many aspects of the indentation process, including the dimensions of the probe and the sample, contact features, and nonlinear material models [24,25]. This method can better capture the response at the large strain range but the computational cost associated with FE models is a drawback for inversely extracting material properties [26]. Furthermore, the number of unknown material parameters needed to identify mechanical behavior and the large amount of experimental data increase the difficulty of the inverse process. In addition, in determining the nonlinear viscoelasticity of biological cells, a complex platform of experimental inputs that is composed of different loading histories might be needed [24,27], contributing to an increased cost in the inverse analysis. In the literature, recent work by [24] employed an inverse FE approach for interpreting AFM experimental data. Nevertheless, details related to these computational issues have still not been thoroughly discussed. Additionally, in many cases of AFM indentation, the experiment is neither force nor displacement controlled because of the manner by which an AFM operates. This is normally neglected during FE modeling, which is also another source of inaccuracy.

This paper focuses on using AFM indentation techniques to investigate the correlation between NLV properties of breast cancer cells (MCF-7 and MCF-10A) and alterations in the cytoskeletal structures utilizing two approaches. In the first, breast cancer cells at the benign (MCF-10A) and malignant (MCF-7) states were indented in their culture medium using spherical probes in AFM contact mode in fluid. A two-step indentation loading input was employed. It was comprised of applying a small force to initiate the contact between the probe and the cell, followed by controlling the AFM piezo movement in a ramp-reverse and ramp-hold manner. In the second, the same indentation procedure was applied to investigate the effect of the drug induced cytoskeletal structure on the cells' NLV characteristics due to a drug treatment with Cytochalasin D. The indentation experiment was simulated using the FE method in which the cell material constitutive relationship is a large strain viscoelastic model. The non-linear elastic part of the material is captured by a hyper-elastic model while the viscoelastic part composes of a two term Prony series to describe the time dependent relaxation. In order to simulate the actual operation in the AFM, the FE model also includes the AFM cantilever in the modeling by using a spring with the same stiffness. Once an FE model is constructed, an inverse analysis is needed to optimize the error between the experimental data and FE predictions. The iterative inverse approach is computationally expensive, as noted in [26]. Therefore an inverse technique based on a surrogate model with the use of a Kriging estimator [27–33] is employed to address this issue. The procedure allows an automatic and efficient extraction of the NLV parameters. The variation of the shear relaxation modulus for each tested cell is, therefore, obtained. Statistical comparisons using the shear relaxation modulus and the amount of relaxation for the two cases (MCF-7 versus MCF-10A, and untreated versus treated MCF-10A) were also conducted to investigate differences in terms of these mechanical properties.

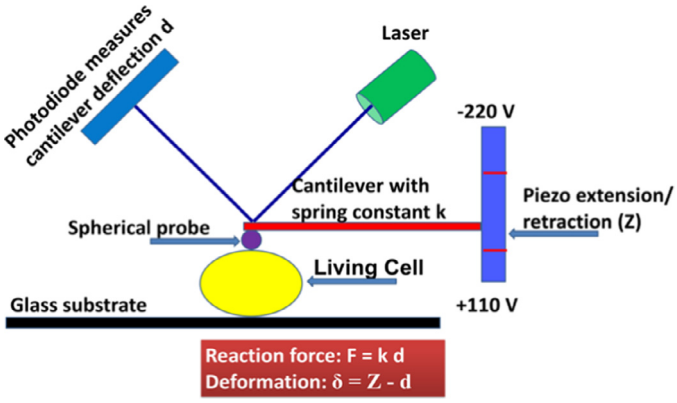

Fig. 1. Illustration of working principle of AFM indentation test on cells.

2. Experiment details

2.1. Sample preparation

Human mammary epithelial cells (MCF-10A) were cultured in mammary epithelial growth medium (MEGM, Lonza) with the GA-1000 replaced by 100 ng/ml cholera toxin (Sigma). Human breast cancer cell line (MCF-7) was maintained in Dulbecco's modified eagle medium (DMEM, Life Technologies) supplemented with 10% fetal bovine serum (FBS, Life Technologies), 1% penicillin/streptomycin (P/S, Life Technologies), 1% fungizone (Life Technologies), and 5 g/ml gentamycin (Life Technologies). For preparing samples for AFM tests, cells were resuspended and seeded onto glass coverslips at density of 40,000–80,000 cells per coverslip. Cells were cultured under 37 °C and 5% CO_2 for at least overnight before any test was performed. For pharmacological treatment assays, MCF-10A cells were incubated with 500 μM Cytochalasin D (Life Technologies) for 2 h and then tested by indentation.

2.2. AFM indentation experiment setup

The working principle of an AFM Bruker Dimension Icon instrument [34] is illustrated in Fig. 1. The sample is fixed to a rigid substrate and compressed by a probe attached to one end of an AFM cantilever (for indenting cells, a spherical probe is often used to reduce damage during the tests). The other end of the cantilever is connected to a piezo. As this piezo extends, the probe moves downward and comes into contact with the sample. On the other hand, as the piezo retracts, the probe moves upward.

Upon contact, the sample's reaction force F causes the cantilever to bend leading to a shift of the laser beam on the photodiode. The amount of shifting is related to the deflection d of the cantilever, which is in turn related to the reaction force by a linear relation $F = kd$. Here, k is the spring constant of the cantilever calibrated using the built-in thermal tune function in the AFM instrument [35]. The deformation δ of the sample is the difference between the piezo distance Z and the cantilever deflection

d: $\delta = Z - d$. With this working principle, the sample's deformation δ, therefore, cannot be controlled. In other words, in the AFM, the control modes can only be either controlling the piezo movement Z or using a feedback loop to control the deflection d, which is correlated to the force F. The first control mode, in which the indentation is performed by ramping and reversing the piezo movement Z, is frequently employed. However, this leads to variations in the loading inputs upon changing samples and setups. In addition, variations in cell heights and properties also contribute to this issue. Therefore, in order to get almost the same input and also to combine many aspects into the loading process, such as loading rate dependencies, hysteresis and relaxation behaviors, the following procedure was employed.

Indentation experiments were performed in a cell culture medium at room temperature using the contact mode in fluid of an AFM Bruker Dimension Icon system (Electron Microbeam Analysis Laboratory, University of Michigan). Before indentation on cells, the deflection sensitivity (DS) for converting the photodiode (or laser) signal of the cantilever deflection from Voltage to *nm* was calibrated by obtaining force curves on a clean glass slide and measuring their slope values. Once the DS value was attained, the thermal tune option [35] was used to measure the cantilever spring constant. The clean glass slide was then replaced by a glass coverslip with the cells seeded on the top. When replacing the coverslip, the laser sum signal was maintained the same to minimize the change in DS value [36]. Next, the spherical indenter was positioned at the center region of each selected cell, and indentation tests were conducted using the script mode, that included two steps as follows:

Step 1: Ramping the set-point (force) to engage the probe on the cell's surface with a small force value (ramp velocity: 1 nm/s, δd = 4 nm, and the applied force value was about 0.3–0.5 nN). This step was to initiate the contact between the probe with the sample's surface. A small value of force was utilized to reduce its effects on the subsequent step, in which the piezo movement (Z) was controlled.

Step 2: A sequence of RR (hysteresis) and RH (relaxation) loading processes, as shown in Fig. 2, was applied to the piezo. It was employed to study the hysteresis as well as relaxation responses of the cells. This loading series consisted of one load–unload cycle at rate 10 μm/s, one load–unload cycle at rate 5 μm/s, and one load–unload cycle at rate 1 μm/s followed by a fast ramp at rate 10 μm/s and a hold period of 50 s. In the first RR cycle, the piezo moved down by an amount of 2 μm, then retracted by an amount of 1 μm. These positions of loading were repeated in the following cycles. These values were chosen to examine a relative large deformation, and also to reduce the negative range of the force–time responses in the unloading paths due to the characteristics of viscoelasticity under displacement control of the AFM piezo. For each cell, the probe was also moved to nearby locations by an offset amounts of 1 μm or 2 μm in order to acquire force–time data at these neighboring positions (2–4 locations per cell were used). In this work, data for each individual cell is the average of these local measurements.

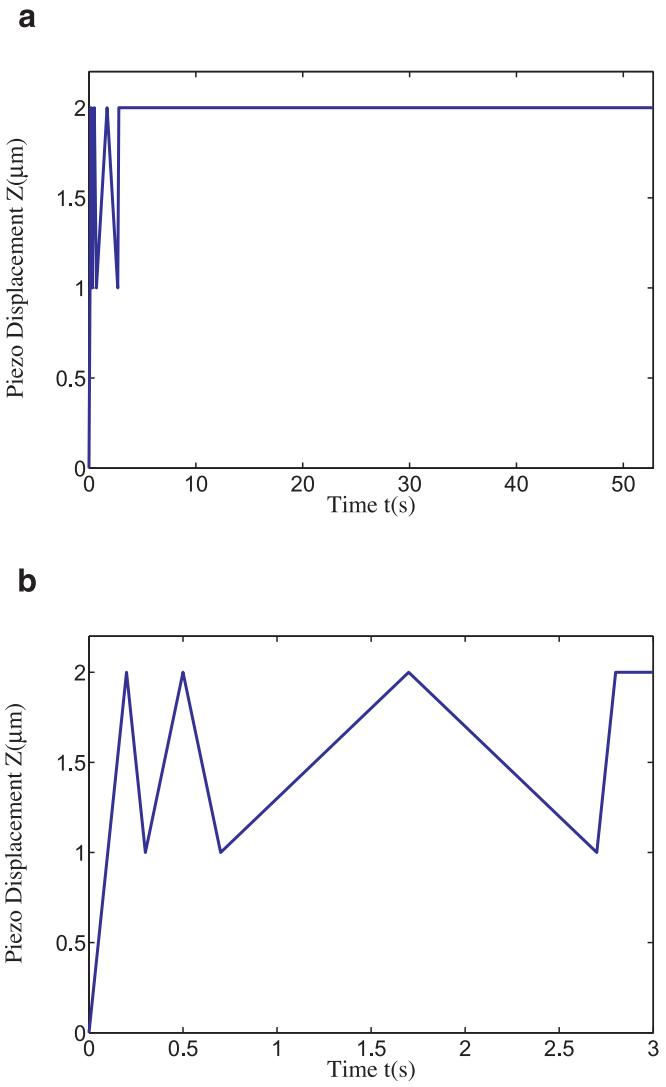

Fig. 2. Applied input Z for controlling the AFM piezo movement: (a) the entire step. (b) Zoom-in view of the RR (ramp-reverse) cycles.

Table 1
Number of breast cancer cells tested in three AFM indentation setups.

Cell groups	Expt. #1	Expt. #2	Expt. #3
MCF-10A (benign)	$n = 23$	$n = 24$	
MCF-7 (malignant)	$n = 23$	$n = 24$	
MCF-10A (untreated)			$n = 17$
MCF-10A (treated)			$n = 17$
k (N/m)	0.120	0.083	0.080
Probe no.	1	2	3

2.3. Experimental data

For the purpose of investigating the roles of viscoelastic properties in establishing biomarkers for cancer detection purpose, two approaches were studied with the described indentation procedure. In the first, experiments were conducted on two groups of benign (MCF-10A) and malignant (MCF-7) cells to study the changes of viscoelastic parameters at different states of breast cancer. In the second approach, the drug Cytochalasin D, which can disrupt the cytoskeleton structure, is used to treat MCF-10A cells. The hypothesis here is that alteration in the cytoskeleton structure, either by cancer transformation [12,13] or by drug treatment [37,38], is correlated with the change in viscoelastic behavior.

Data obtained from three setups is presented to validate this hypothesis. Table 1 is a summary of the number of cells tested as well as the value of the calibrated spring constant of the cantilever used in each setup.

Mean and standard deviations for MCF-10A and MCF-7 groups from the first setup are shown in Fig. 3. The top figure shows the force–time responses for both RR (hysteresis) and RH (relaxation) loading types. The bottom one is a zoom-in view of the force–time behavior in RR (hysteresis) cycles. Similarly, Fig. 4 presents the mean and standard deviations for MCF-10A and MCF-7 groups acquired from the second setup. Data obtained from the drug

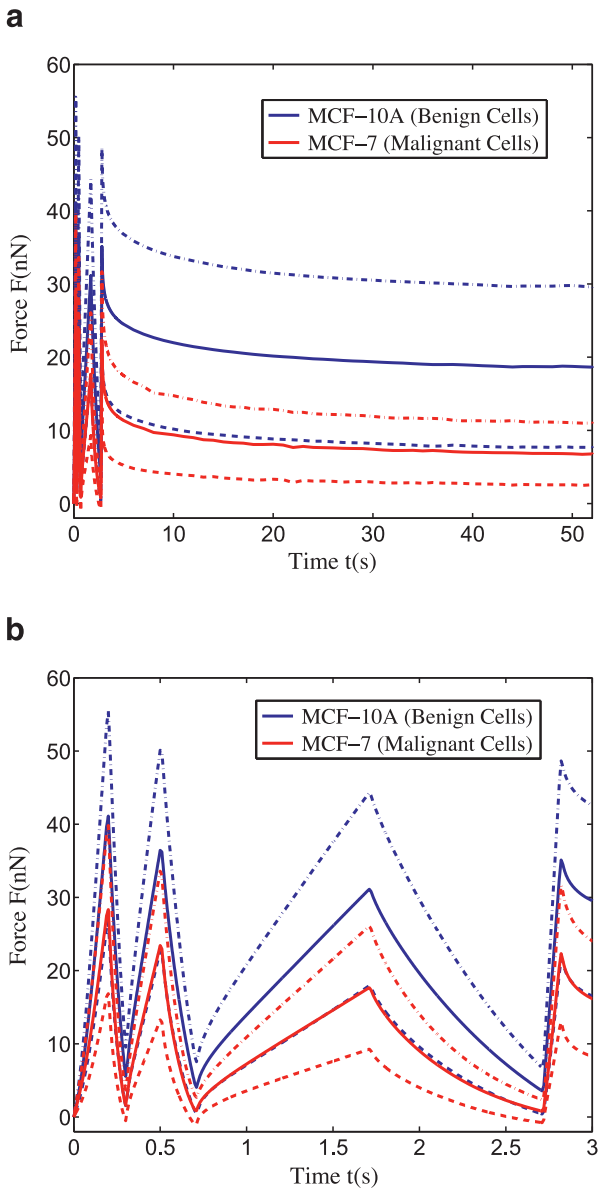

Fig. 3. AFM experimental data (mean and standard deviations) for MCF-10A and MCF-7 cells obtained in the first setup: (a) both RR (ramp-reverse) and RH (ramp-hold) responses. (b) Zoom-in view of the RR (ramp-reverse) responses.

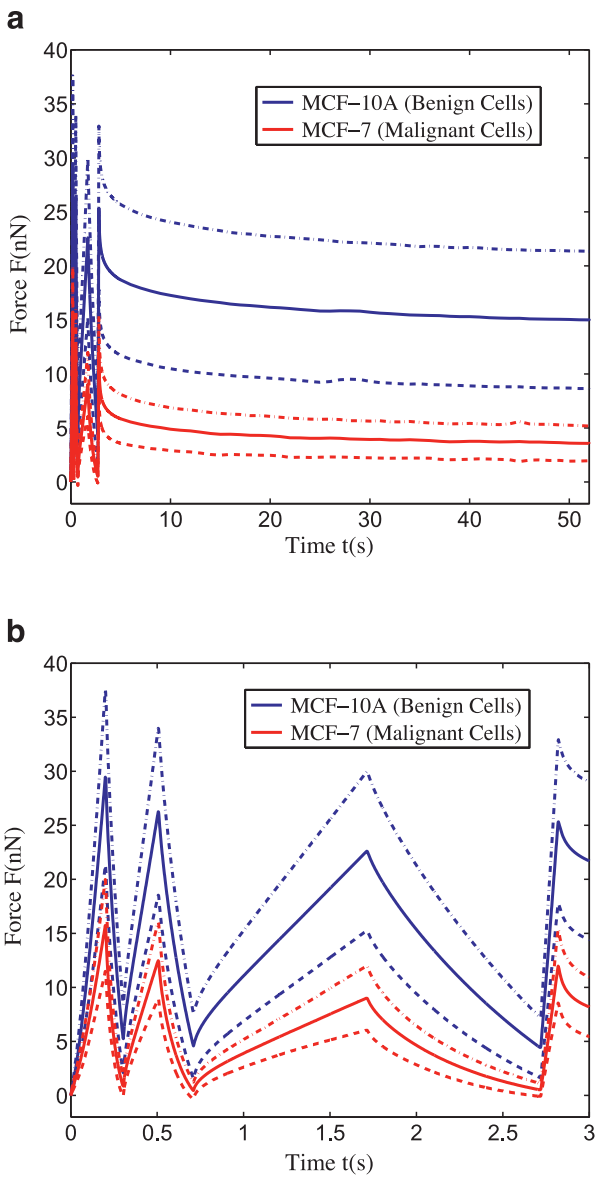

Fig. 4. AFM experimental data (mean and standard deviations) for MCF-10A and MCF-7 cells obtained in the second setup: (a) both RR (ramp-reverse) and RH (ramp-hold) responses. (b) Zoom-in view of the RR (ramp-reverse) responses.

treatment approach is presented in Fig. 5 which includes the mean and standard deviations for the untreated MCF-10A cells as compared to the treated cells. Due to the nature of biological cells, large variations were observed. Additionally, the magnitudes of the peak forces are significantly influenced by the loading rates. As shown in Figs. 3–5, in all three setups, the peak force value drops as the loading rate decreases. This suggests a relaxing behavior of the cell, which also corresponds to the relaxation parts during the ramp-hold (RH) periods.

For a preliminary, qualitative comparison, each force–time curve is normalized by the value of its maximum peak force. The corresponding normalization data from these setups is plotted in Figs. 6–8. As observed in Fig. 6, the force–time responses of MCF-7 cells exhibited more relaxation than the ones obtained from MCF-10A cells. Specifically, at the end of the loading range, the mean force–time of the MCF-10A group dropped by about 57.72%, while an amount of about 76.86% was seen in the MCF-7 group. This trend is also observed in Fig. 7. Here, the mean force–time of the MCF-10A group decreased by about 50.62% as compared to about 77.19% drop in MCF-7 group. Similarly, the treated MCF-10A group also experienced more relaxation than the untreated MCF-10A group. Data presented in Fig. 8 showed that, at the end of the loading range, the decreases in the force–time responses for the untreated and treated groups were about 53.13% and 87.23%, respectively. These may imply that changes in the cytoskeleton, either due to disease states or a drug treatment, can be correlated with the viscoelastic (history-dependent) properties, especially the relaxation characteristics.

3. FE modeling

The FE method with the commercial code ABAQUS [39] was employed to model the two-step indentation process described in Section 2.2. The seeded cell was assumed to be an isotropic, homogenized, axisymmetric body having an oblate-shape with a circular base [26]. For each tested cell, the diameter of the base was estimated as the square root of the product of two representative

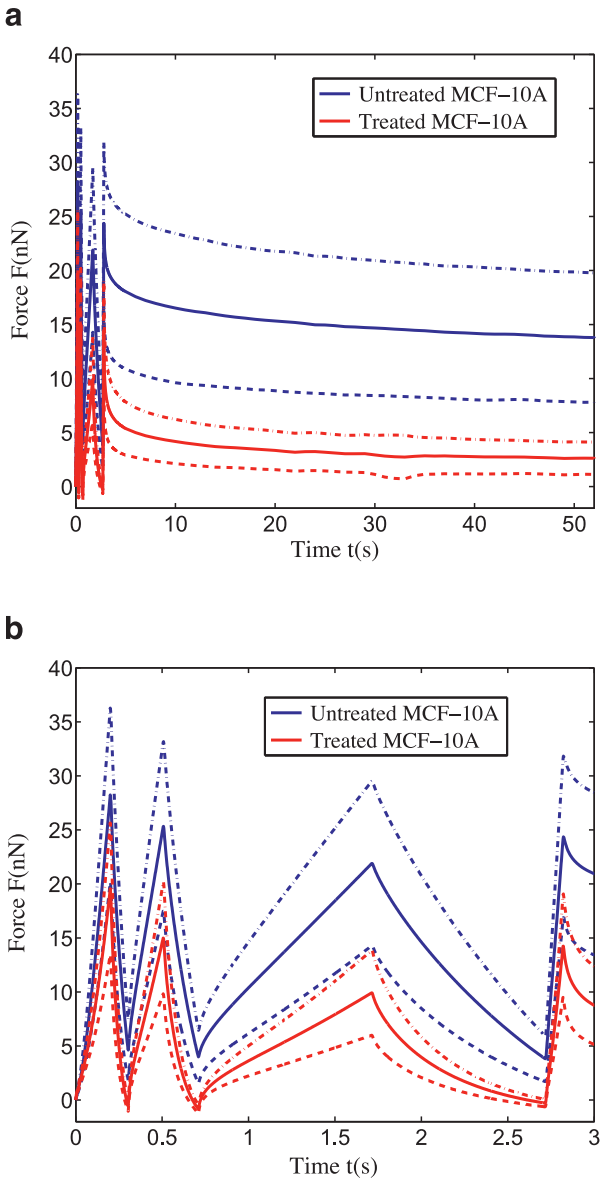

Fig. 5. AFM experimental data (mean and standard deviations) for MCF-10A cells, untreated and treated with the drug Cytochalasin D, obtained in the third setup: (a) both RR (ramp-reverse) and RH (ramp-hold) responses. (b) Zoom-in view of the RR (ramp-reverse) responses.

distances taken from its optical images [24]. A typical image for a tested cell is shown in Fig. 9. The cell height was estimated using the contact points of force-curves on the cell body and on the nearby glass surface [24]. For this purpose, after the measurements using the above two-step indentation process were conducted, the typical indentation procedure, in which the AFM ramp mode was used to ramp the piezo movement in a ramp-reverse loading, was also performed to acquire the force curves on specified locations of the cell body and the glass coverslip's surface. A trigger value of 50 nm was selected to limit the amount of the maximum cantilever deflection, which corresponded to a limit value of about 4–6 nN for the maximum applied force. A typical comparison between force curves on the cell body and on the glass substrate is shown in Fig. 10. The difference between the two contact points gives an estimation for the cell height.

For the first setup, an axisymmetric FE model for a representative cell, using the mean height and diameter values of $H = 12.22$ μm and $D = 28.88$ μm, was used to simulate the

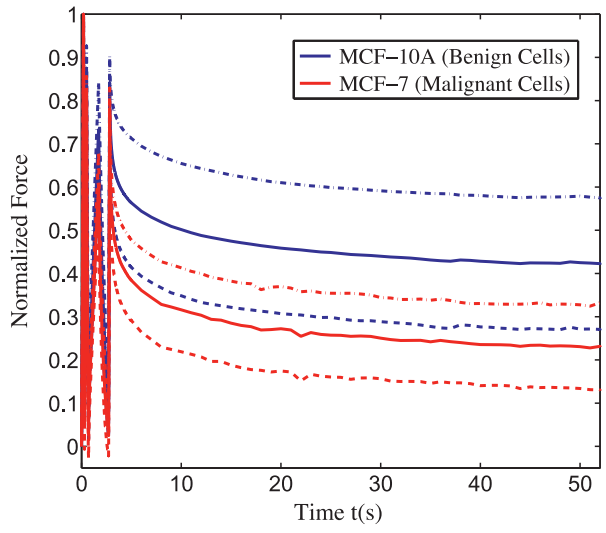

Fig. 6. Normalization by the peak force for MCF-10A and MCF-7 cells (first setup).

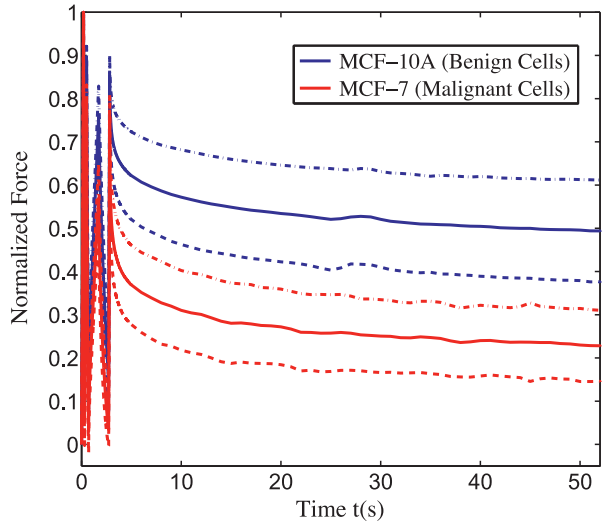

Fig. 7. Normalization by the peak force for MCF-10A and MCF-7 cells (second setup).

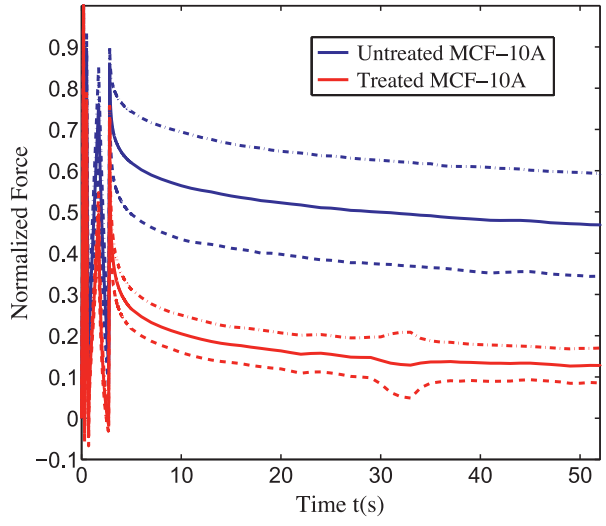

Fig. 8. Normalization by the peak force for MCF-10A cells and MCF-10A cells treated with the drug Cytochalasin D (third setup).

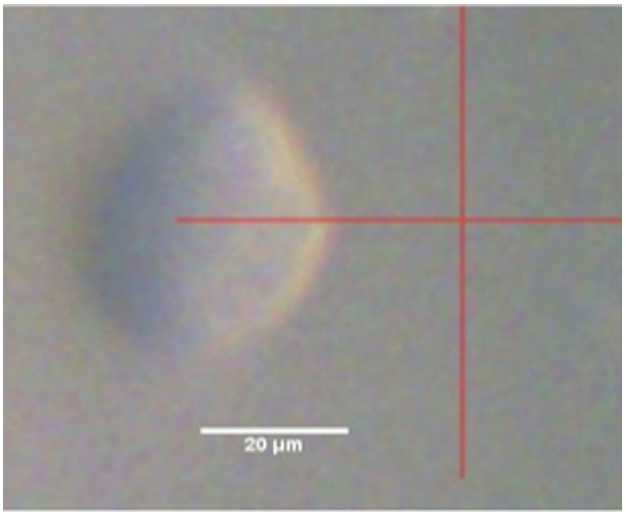

Fig. 9. An optical image of a single breast cancer cell on a glass substrate captured by the optical microscopy in an AFM Bruker Dimension Icon.

indentation process. The cantilever with the spherical probe was modeled as a spring connected to a rigid sphere of diameter 5 μm. The spring stiffness was set equal to the calibrated value obtained from the AFM experiments, which was 0.12 N/m in this case. The spherical probe was modeled as a rigid body. Its contact with the cell was assumed to be frictionless, and the normal behavior was modeled by the hard contact option in ABAQUS. The entire procedure of the two-step indentation as described in Section 2.2 was simulated, in which the input was applied to the free end of the spring. The cell deformation was extracted as the displacement of the other end of the spring. The difference between the displacements of these two ends of the spring is how much the cantilever bends during the indentation process, and is related to the reaction force by the linear relation: $F = kd$. The boundary conditions of the problem were imposed by fixing the bottom surface with the assumption that the cells attach firmly to the coverslip. This approach was also used to model the indentation processes in the other two setups. Specifically, for the second setup, the dimensions of the representative cell were $H = 11.96$ μm and $D = 31.00$ μm, and the spring constant stiffness was 0.083 N/m. For the third setup, these values were $H = 8.84$ μm, $D = 27.63$ μm, and $k = 0.080$ N/m. Convergence studies were also performed by varying the mesh size of each model. Three cases of meshing used for the first setup are illustrated in Fig. 11. The numbers of total elements are: (a) 1192, (b) 4213, and (c) 16,582. The force–time responses from the last two mesh sizes were converged, and were only slightly different from the response obtained from the first mesh. In this work, the middle mesh size was used to simulate the indentation for the first setup. The same process was applied to determine the optimum mesh size in modeling the second and the third setups.

4. Results and discussions

4.1. Implementation of the inverse analysis

At a relatively large imposed displacement (Fig. 2), the cell behavior is better captured using a non-linear constitutive relation. Here, the built-in NLV model in ABAQUS presented in Section 4.8-2 of ABAQUS Theory Manual version 6-10 [39] was employed to describe the time-dependent behavior of the cells. For simplicity, a neo-Hookean type model for the nonlinear elastic part was utilized. With the incompressibility assumption, for each tested cell, five unknown material parameters need to be characterized, and its shear relaxation modulus as a function of time is constructed as follows:

$$G(s) = G_\infty + \sum_{k=1}^{2} G_k e^{-s/\tau_k} = G_0 \left[g_\infty + \sum_{k=1}^{2} g_k e^{-s/\tau_k} \right], \tag{1}$$

where $G_0 = G(0)$ is the instantaneous shear modulus, which also has the meaning of the neo-Hookean parameter C_1, is used to capture the nonlinear elastic part. $G_\infty = G(\infty)$ is the long term shear modulus of the cell at its totally relaxed (long term equilibrium) state. $g_\infty = G_\infty/G_0$ is the ratio between the long term and instantaneous shear moduli. The relaxation process of the cell is described using two term Prony series (g_k, τ_k), $k = \overline{1,2}$. Here $g_k = G_k/G_0$ for $k = \overline{1,2}$ are dimensionless quantities associated with the relative changes in the amount of relaxation. Note that $g_1 + g_2 + g_\infty = 1$, thus $g_1 + g_2 < 1$. τ_k, $k = \overline{1,2}$ are the relaxation times which describe how fast the relaxation is.

The inverse analysis based on surrogate modeling with a Kriging estimator [28–33] was employed. Details about the implementation of this analysis for extracting NLV properties from experimental data were presented in [27]. For brevity, only the main steps in the inverse procedure are included in this paper.

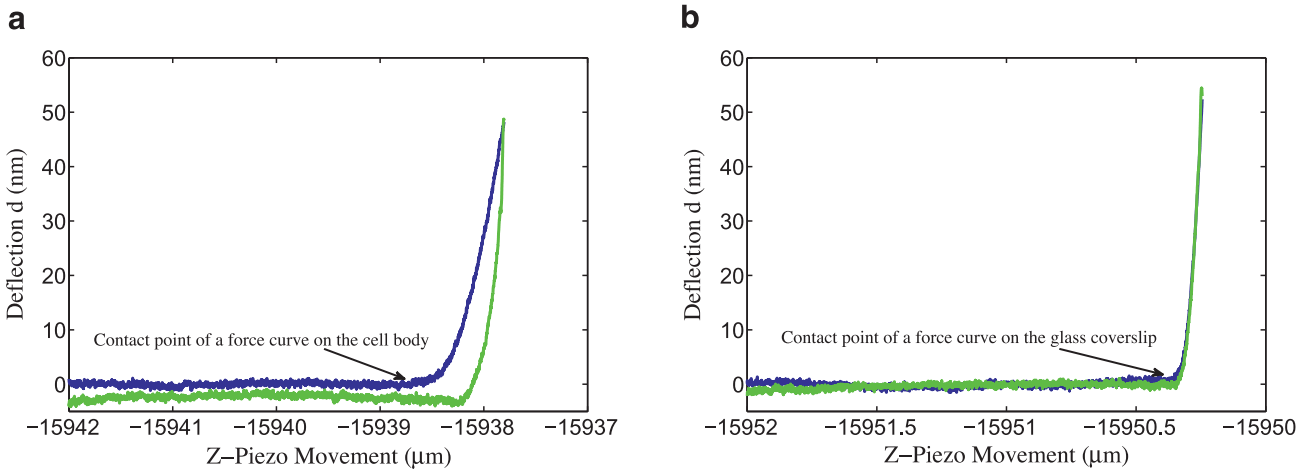

Fig. 10. Cantilever deflection versus the piezo movement (with the reference corresponds to the highest location of the scanner): (a) on a breast cancer cell body and (b) on the glass surface. The difference between the two contact points gives an estimation of the cell height. The contact point was visually determined as the point at which the deflection deviates from its horizontal baseline.

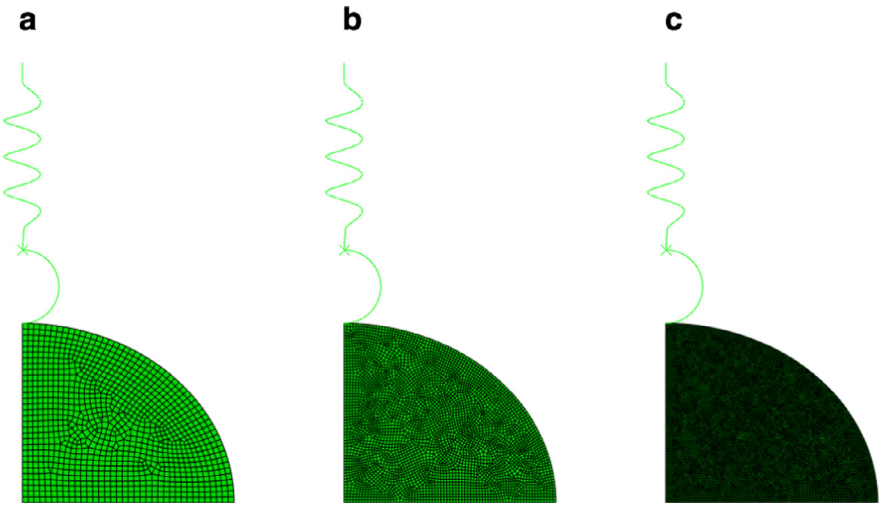

Fig. 11. FE model for an AFM indentation test on breast cancer cells with three cases of meshing: (a) 1192 elements, (b) 4213 elements, and (c) 16,582 elements.

Table 2
Boundary of the material domain used in the process of determining the NLV properties of the tested breast cancer cells in three setups.

	C_1(kPa)	g_1	τ_1(s)	g_2	τ_2(s)
Lower bound	0.08	0.01	0.01	0.01	2
Upper bound	4	1	2	1	40

The material properties for all tested cells were searched within the material domain given in Table 2.

For each FE model discussed in Section 3, within the given material domain, the MATLAB's function "*lhsdesign*", in which the Latin Hypercube sampling technique was implemented, was applied to generate N and N^1 sets of material properties for a training group and a checking group, respectively. With the condition that $g_1 + g_2 < 1$, a training group composed of $N = 970$ sets of $x^i(G_0, g_1, \tau_1, g_2, \tau_2)$, $i = \overline{1, N}$ was used in this work. A checking group composed $N^1 = 354$ sets of $x^i(G_0, g_1, \tau_1, g_2, \tau_2)$, $i = \overline{1, N^1}$, which are different from the sets in the training group, was also generated. Since these sets of material parameters are independent, FE simulations were evaluated and the corresponding force–time responses were extracted in parallel. In this work, each force–time response was represented by $m = 5095$ discrete times, which were used to discretize the total loading time in the ramp-reverse and ramp-hold cycles. Specifically, $N = 970$ sets of $(t_j, F(t_j))$, $j = \overline{1, m}$ and $N^1 = 354$ sets of $(t_j, F^1(t_j))$, $j = \overline{1, m}$ were obtained for the training and checking groups, respectively. In other words, the training group has $N = 970$ sets of material parameters $x^i(G_0, g_1, \tau_1, g_2, \tau_2)$, $i = \overline{1, N}$, which correspond to $N = 970$ sets of force values $y^i(F(t_j))$, $i = \overline{1, N}$, $j = \overline{1, m}$. Similarly, the checking group contains $N^1 = 354$ sets of material parameters $x^i(G_0, g_1, \tau_1, g_2, \tau_2)$, $i = \overline{1, N^1}$, which correspond to $N^1 = 354$ sets of force values $y^i(F^1(t_j))$, $i = \overline{1, N^1}$, $j = \overline{1, m}$. The MATLAB's Dace Toolbox [29] is, therefore, applied to the training group to construct a non-linear functional relationship between $X(5, 970)$ and $Y(5095, 970)$. Its accuracy is checked through the checking group $X^1(5, 354)$ and $Y^1(5095, 354)$. For the specific problem considered here, since no experimental force–time curve obtained in the three setups has a peak force value smaller than 4 nN, an extra criterion is utilized to remove the force responses which violate this observation in both training and checking groups. This extra criterion is used to help the construction of the surrogate model easier and reduce the need of adding more training points. Typically, with this criterion, about 4–10 cases were removed from the training group, and about 2–5 were removed from the checking group. The specific numbers depend on the FE model used in generating the surrogate model. For brevity, this section only discusses the surrogate model and the Kriging predictor constructed using one particular FE model from the first setup. Surrogate models and Kriging predictor for other FE models were also constructed using the described procedure [27–33].

In particular, a surrogate model with a Kriging predictor was constructed, using the FE model for a representative cell of $H = 12.22$ μm and $D = 28.88$ μm (first setup). It is a non-linear relationship between sets of material properties $X(5, 962)$ and sets of the corresponding force responses $Y(5095, 962)$. The accuracy of this Kriging predictor was verified through the checking group, which is composed of $X^1(5, 349)$ and $Y^1(5095, 349)$. For these 349 cases, the root mean square error (RMSE) values were evaluated as follows:

$$RMSE(i) = \frac{1}{range(y^i_{FE})}\sqrt{\frac{1}{5095}\sum_{k=1}^{5095}(y^i_{FE(k)} - y^i_{Krg(k)})^2}. \quad (2)$$

These values range from 0.03% to 8%. Representative comparisons between the actual FE responses and the predictions obtained by Kriging predictor are shown in Fig. 12. As shown in this figure, many predictions from Kriging overlayed with the actual FE responses, and the differences between the two corresponding curves (red and blue) are not visible in this plot.

Notice that evaluations using Kriging predictor is much faster than using FE simulations. It is therefore used to replace FE simulation in the property extraction process to reduce the computational cost of the optimization process. Specifically, the error between the obtained experimental data with predictions from Kriging predictor is optimized using the MATLAB's function *fmincon* to extract sets of optimized material properties. FE simulations were also evaluated at these extracted sets of material properties and then were compared with the experimental data to determine the quality of the extracted sets of properties. Representative comparisons between the experimental data and FE evaluations using the optimized sets of material properties from this inverse procedure are presented in Fig. 13.

As shown in Fig. 13, predictions from FE captured quite well the complicated responses of the experimental data from five individual MCF-10A cells in the first setup. The RMSE values for these

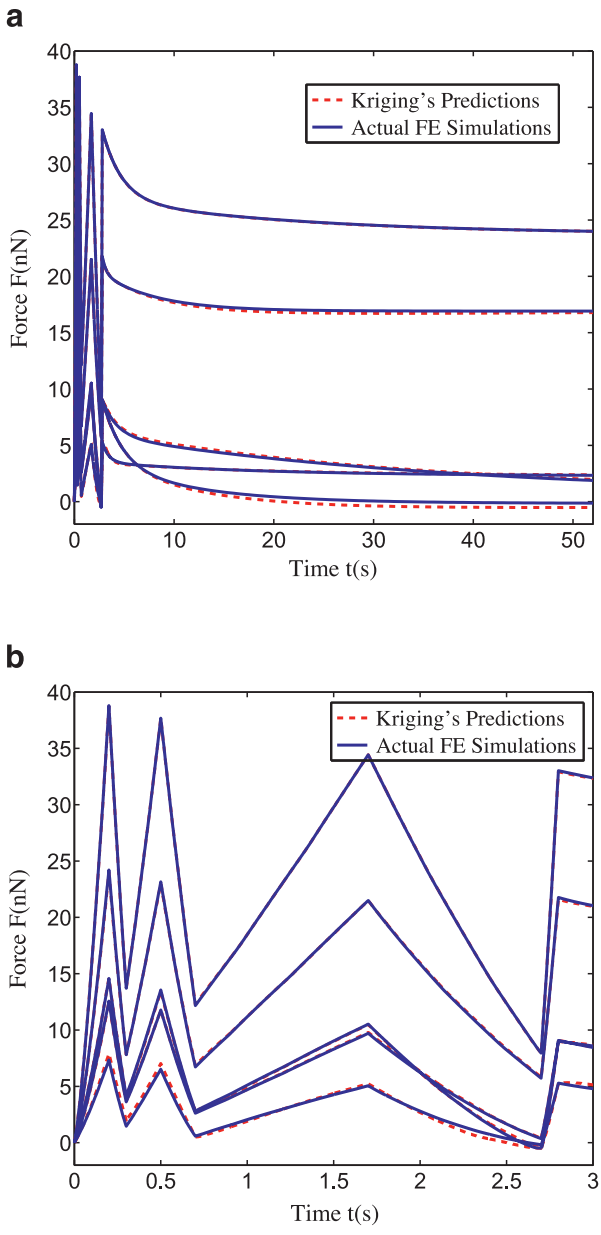

Fig. 12. Representative comparisons between FE and Kriging predictions: (a) both RR (ramp-reverse) and RH (ramp-hold) loadings. (b) Zoom-in view of RR (ramp-reverse) cycles. (For interpretation of the references to color in this figure legend, the reader is referred to the web version of this article.)

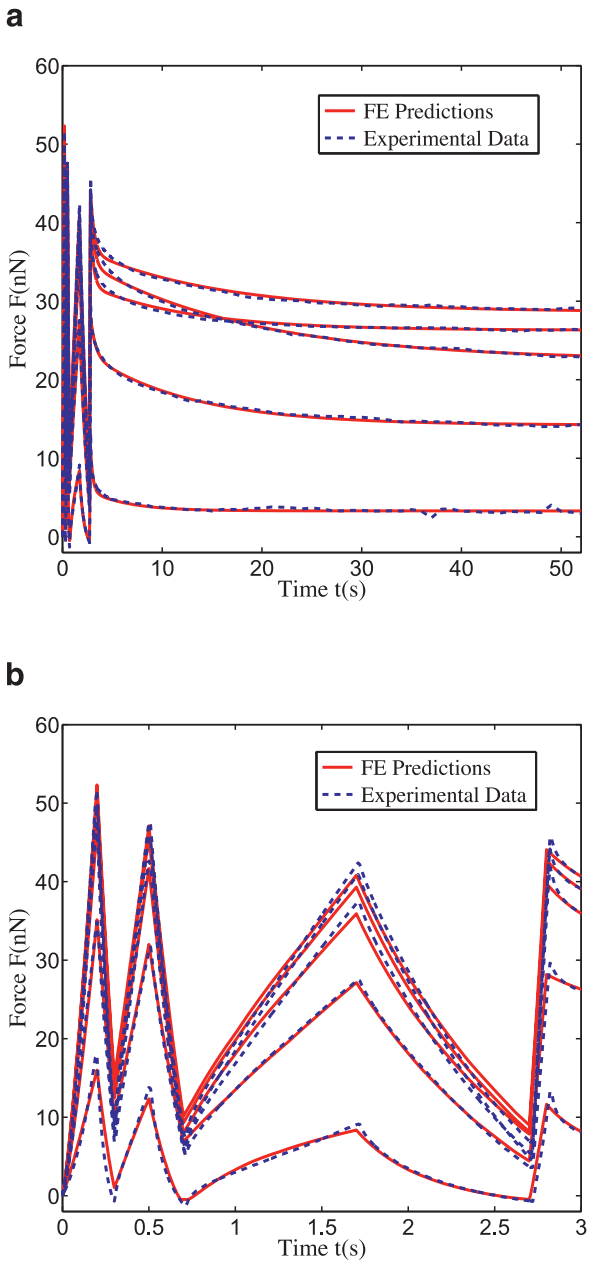

Fig. 13. Representative comparisons between experimental data and FE predictions at the corresponding extracted sets of material parameters: (a) both RR (ramp-reverse) and RH (ramp-hold) loadings. (b) Zoom-in view of RR cycles.

fittings were evaluated as follows:

$$RMSE(i) = \frac{1}{range(y^i_{exp})}\sqrt{\frac{1}{5095}\sum_{k=1}^{5095}(y^i_{FE(k))} - y^i_{exp(k)})^2}. \quad (3)$$

Such values for fitting the data obtained from $n = 23$ MCF-10A and $n = 23$ MCF-7 cells of the first setup lie between 2% and 8%, with a mean value of about 4%. This indicates reasonable agreement between FE predictions and experimental data from all tested cells. With the same approach, NLV properties were also extracted from the experimental data from the other two setups.

At this step, an optimal set of five NLV parameters (G_0, g_1, τ_1, g_2, τ_2) was extracted for each tested cell. For comparison purposes, the shear relaxation moduli were constructed using Eq. (1). Results are discussed in detail in the next section.

4.2. Discussion, limitations, and concluding comments

Shear relaxation moduli for MCF-10A and MCF-7 cells measured in the first setup are shown in Fig. 14(a). Here, the instantaneous shear modulus values for MCF-10A cells are $G(0) = 2.94 \pm 1.35$ kPa as compared to $G(0) = 1.94 \pm 1.02$ kPa obtained for MCF-7 cells. The mean results of the instantaneous shear modulus indicate that MCF-10A cells are about 1.5 times stiffer than MCF-7 cells at the instantaneous response. At the long term response, such as at the end of the loading, $t = 52$ s, the shear modulus values for MCF-10A and MCF-7 cells obtained in this setup are $G(52) = 1.00 \pm 0.64$ kPa and $G(52) = 0.36 \pm 0.21$ kPa, respectively. The mean results of this long-term shear modulus indicate a larger difference of 2.8 times as compared to the corresponding instantaneous values. To further determine whether the observed differences here are significant or not, statistical comparisons using

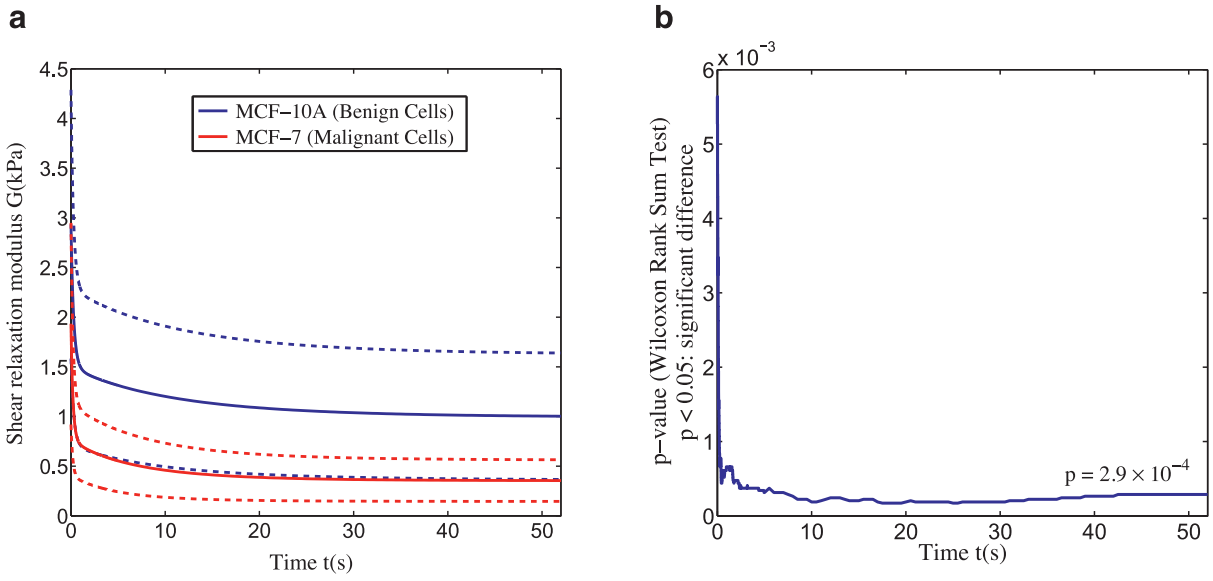

Fig. 14. Comparisons between MCF-10A and MCF-7 cells (in the first setup): (a) mean and standard deviations of the shear relaxation modulus for $n = 23$ MCF-10A (blue) and $n = 23$ MCF-7 (red) cells. (b) Statistical comparison: $p < 0.05$ indicates significant difference. (For interpretation of the references to color in this figure legend, the reader is referred to the web version of this article.)

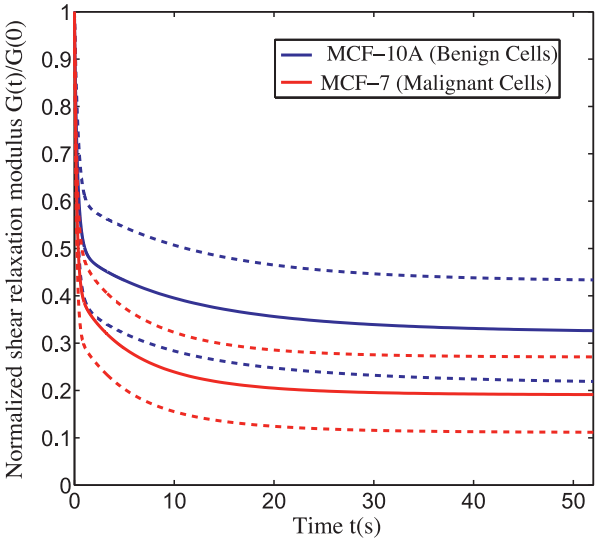

Fig. 15. Mean and standard deviations of the normalized shear relaxation modulus $G(t)/G(0)$ for MCF-10A and MCF-7 cells (in the first setup).

the Wilcoxon rank sum test in MATLAB are used. Fig. 14(b) shows that the two groups exhibit significant differences in terms of the shear relaxation modulus. The difference becomes more significant at the long term response. Such results indicate that combining the history-dependent characteristics into the calculations of the shear relaxation modulus might help to rule out larger difference between these two cell groups.

In addition to the shear relaxation modulus, the amount of relaxation $G(t)/G(0)$ can also be compared between two groups. Fig. 15 shows the mean and standard deviation of the normalized shear relaxation modulus for both groups. In this case, the mean amount of relaxation for the MCF-10A group is about 67%, while an amount of about 81% is found for the MCF-7 group. At the end of the loading, statistical analysis using the MATLAB Wilcoxon rank sum test also indicates a significant difference in the amount of relaxation between the two groups ($p = 1.2 \times 10^{-4}$).

Similar observations were also obtained from the analysis of the data taken from the second setup. As shown in Fig. 16(a), at each time, the shear relaxation modulus of the MCF-10A group exhibits a higher value than the modulus of the MCF-7 group. The statistical analysis also results in a significantly small p-value for the comparisons using the shear moduli of both groups. Again, the p-value becomes smaller at the long term response which might be attributed to the incorporation of viscoelasticity in the calculation of the shear relaxation modulus function. MCF-7 group also exhibits a larger amount of relaxation as compared to the MCF-10A group as presented in Fig. 17. Specifically, the mean shear relaxation modulus for the MCF-7 group drops by 78%, while the shear modulus for the MCF-10A group decreases by 57% at the end of the loading. The p-value for this case is $p = 9.7 \times 10^{-7}$, which means the difference in terms of the amount of relaxation is significant as well.

So far, the results obtained for MCF-10A and MCF-7 cells from both setups exhibit a similar trend for the relative difference between these two cell groups. The benign cells (MCF-10A) are stiffer and exhibit less relaxation than the malignant (MCF-7) cells. By considering viscoelasticity in the characterization of the shear modulus, the relative difference between them are also exhibited in terms of the long-term shear modulus. The data exhibited a larger difference in the long term response as compared to the corresponding difference in the instantaneous behavior.

Next, the data obtained for the untreated and treated MCF-10A cells using the drug Cytochalasin D are also compared. Fig. 18(a) shows the difference of the shear relaxation modulus between the two groups. Treating MCF-10A cells by the drug Cytochalasin D does lead to a decrease in the stiffness. The difference is amplified in the long term response. As shown in Fig. 18(b), the p-value drops drastically from the instantaneous to long term responses. Here, the plot was presented only up to a time $t = 3$ s for clarity. This agrees with the large difference in terms of the amount of relaxation obtained from these two cell groups. Specifically, at the end of the loading, the mean shear modulus of the untreated group decreases by about 60%, while the mean value of the treated group drops by about 89% (Fig. 19). The p-value for this difference is $p = 1.2 \times 10^{-6}$.

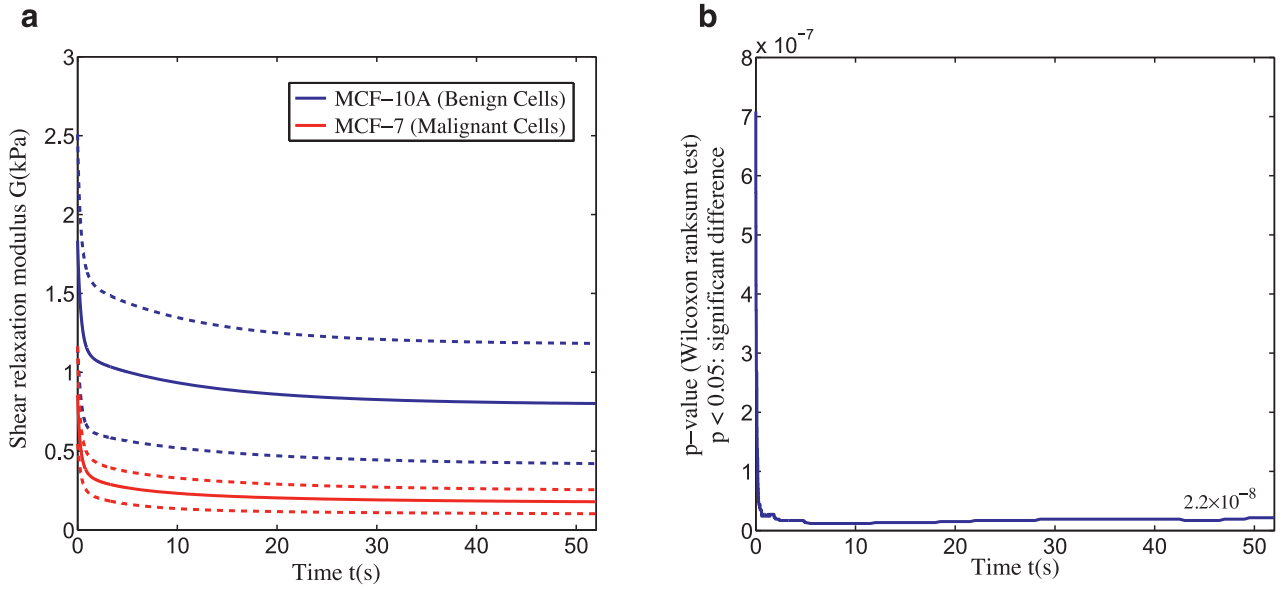

Fig. 16. Comparisons between MCF-10A and MCF-7 cells (in the second setup): (a) mean and standard deviations of the shear relaxation modulus for $n = 24$ MCF-10A (blue) and $n = 24$ MCF-7 (red) cells. (b) Statistical comparison: $p < 0.05$ indicates significant difference. (For interpretation of the references to color in this figure legend, the reader is referred to the web version of this article.)

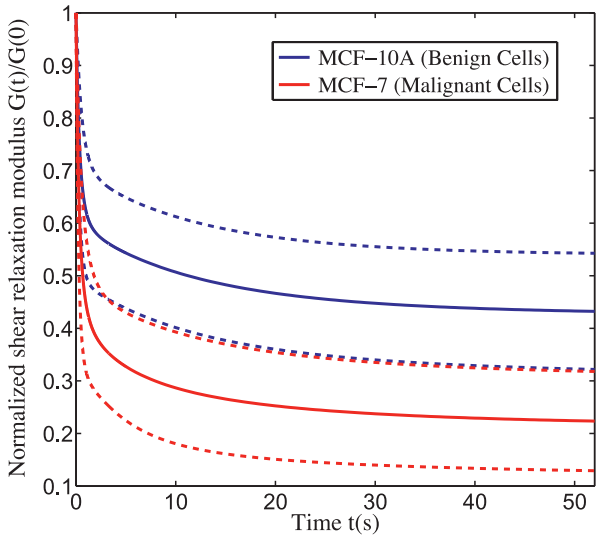

Fig. 17. Mean and standard deviations of the normalized shear relaxation modulus $G(t)/G(0)$ for MCF-10A and MCF-7 cells (in the second setup).

The above analysis focuses only on the relative differences between two cell groups within one setup. The benign cells (MCF-10A) exhibit higher shear relaxation modulus statistically, as compared to the malignant cells (MCF-7). The amount of relaxation is also useful to distinguish these two groups of cells. Transformation into the malignant state might contribute to more relaxation in the response of the malignant cells. Disrupting the cytoskeleton of the MCF-10A cells also causes a drop in both shear relaxation modulus and an increase in the amount of relaxation. These relative differences were found to be consistent from setup to setup, which means that under the same experimental condition, including viscoelastic characteristics into the determination of the material properties proves helpful in providing more insight to differentiate different cell groups for disease detection purpose. Though the absolute values are not reliable [40], the values for the shear relaxation modulus for MCF-10A and MCF-7 cells found in this work are within the range reported in the literature. For example, [12,13] reported the range for Young's modulus of MCF-7 cells to be 0.3–0.6 kPa, and the modulus of MCF-10A to be 1.4–1.8 times stiffer; [41] reported the values in the range 15–30 kPa for MCF-7 cells; and the value in the work of [37] for MCF-7 cells is 4.7 ± 0.4 kPa. In this work, a combination of three setups provides a prediction of the instantaneous modulus of $E(0) = 3G(0) = 6.5 \pm 3.3$ kPa and $E(0) = 3G(0) = 4.2 \pm 2.7$ kPa for $n = 64$ MCF-10A and $n = 47$ MCF-7 cells, respectively. The predictions for the long term modulus, at $t = 52$ s, are $E(52) = 3G(52) = 2.5 \pm 1.5$ kPa and $E(52) = 3G(52) = 0.8 \pm 0.5$ kPa for $n = 64$ MCF-10A and $n = 47$ MCF-7 cells, respectively.

The following limitations and sources of errors are noted in order to further investigate NLV aspects of living cells and evaluate whether the above differences could be adopted for clinical use. Among these limitations, several are related to experimental issues, including the uncertainty in determining the contact points between cell body and the probe, cell geometric determination, and errors in the AFM calibrations. For example, an error of about 10–20% could be associated with the calibration of deflection sensitivity and spring constant [42,43]. In addition, the optical resolution in the AFM Dimension Icon system should be enhanced for better estimations of the cell dimensions and shapes. Having a higher optical resolution also aids the selections of the cells for indentation purposes. This might help to reduce scatter due to geometry effects in the measured data. This issue could be addressed using an AFM system that has an inverted optical microscopy. Such a system is the MFP 3D, manufactured by Asylum Research. Other sources, such as the resolution and backlash in the Z-stepper motor intrinsic mechanical design might cause error in cell height determination. Unintended delay can happen in running a script with high loading rates, such as in the first ramp-reverse cycle at the rate of 10 μm/s. This contributes to an artifact in the acquisition of the force responses. For instance, instead of having a sharp peak force between the loading and unloading paths, a delay of the piezo might occur and cause unintended relaxation in the force–time response. A possible reason for this issue is the clogging up of the messaging in the computer operation. Additionally, as a cell is dynamic and heterogeneous, the model considered here is still a very simple model. Though the NLV constitutive model with Prony

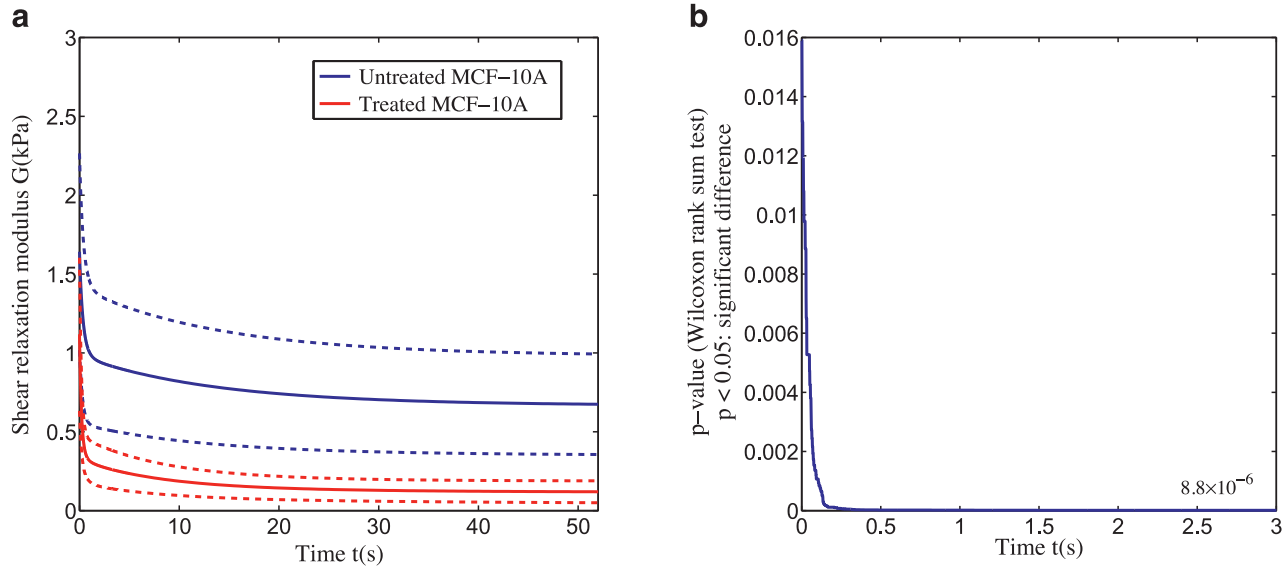

Fig. 18. Comparisons between the untreated MCF-10A cells and MCF-10A cells treated with the drug Cytochalasin D (in the third setup): (a) mean and standard deviations of the shear relaxation modulus for $n = 17$ untreated MCF-10A (blue) and $n = 17$ treated MCF-10A (red) cells. (b) Statistical comparison: $p < 0.05$ indicates significant difference. (For interpretation of the references to color in this figure legend, the reader is referred to the web version of this article.)

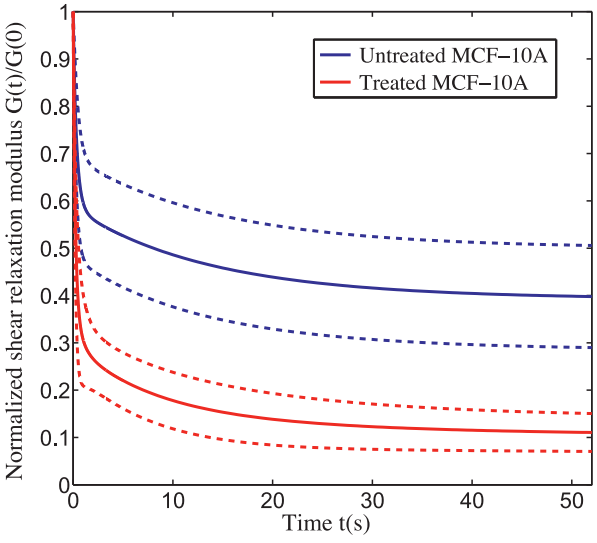

Fig. 19. Mean and standard deviations of the normalized shear relaxation modulus $G(t)/G(0)$ for untreated and treated MCF-10A cells (in the third setup).

series terms was able to capture various aspects of the responses, such as loading rate dependencies and relaxation characteristics, further refinement is necessary. For instance, the response associated with high rate loading and transition between various loading rates, if improved, is expected to lead to better agreement with the experimental data. Furthermore, improvements can be made to enhance the accuracy of the current surrogate modeling and Kriging predictor, including adding more training points in the design site.

In summary, this paper presents a methodology to study the NLV properties of breast cancer cells. Experimental data was acquired at a large strain regime incorporating many aspects, such as non-linear mechanics, rate dependency, and history-dependent characteristics. The data was analyzed using FE models and inverse modeling in connection with surrogate modeling and a Kriging predictor to resolve the computational cost issue. Comparisons were made based on the extracted shear relaxation modulus and results indicated significant differences in terms of the NLV responses between MCF-10A and MCF-7 cells as well as between untreated and treated MCF-10A cells.

References

[1] W.M. Kühtreiber, R.P. Lanza, W.L. Chick, Cell Encapsulation: Technology and Therapeutics, Birkhäuser, Boston, 1999.
[2] G. Bao, S. Suresh, Cell and molecular mechanics of biological materials, Nat. Mater. 2 (2003) 715–725.
[3] H. Karcher, J. Lammerding, H. Huang, R.T. Lee, R.D. Kamm, M.R. Kaazempur–Mofrad, A three-dimensional viscoelastic model for cell deformation with experimental verification, Biophys. J. 85 (2003) 3336–3349.
[4] S. Suresh, J. Spatz, J.P. Mills, A. Micoulet, M. Dao, C.T. Lim, M. Beil, T. Seufferlein, Connections between single-cell biomechanics and human disease states: gastrointestinal cancer and malaria, Acta Biomater. 1 (1) (2005) 15–30.
[5] S. Suresh, Mechanical response of human red blood cells in health and disease: some structure-property-function relationships, J. Mater. Res. 21 (8) (2006) 1871–1877.
[6] M.R.K. Mofrad, R.D. Kamm, Cytoskeleton Mechanics, Cambridge University Press, New York, 2006.
[7] S. Suresh, Biomechanics and biophysics of cancer cells, Acta Biomater. 3 (4) (2007) 413–438.
[8] S.E. Cross, Y. Jin, J. Rao, J.K. Gimzewski, Nanomechanical analysis of cells from cancer patients, Nat. Nanotechnol. 2 (2007) 780–783.
[9] M. Prabhune, G. Belge, A. Dotzauer, J. Bullerdiek, M. Radmacher, Comparisons of mechanical properties of normal and malignant thyroid cells, Micron 43 (12) (2012) 1267–1272.
[10] J. Guck, S. Schinkinger, B. Lincoln, F. Wottawah, S. Ebert, M. Romeyke, D. Lenz, H.M. Erickson, R. Ananthakrishnan, D. Mitchell, J. Käs, S. Ulvick, C. Bilby, Optical deformability as an inherent cell marker for testing malignant transformation and metastatic competence, Biophys. J. 88 (25) (2005) 3689–3698.
[11] E.C. Faria, N. Ma, E. Gazi, P. Gardner, M. Brown, N.W. Clarke, R.D. Snook, Measurements of elastic properties of prostate cancer cells using AFM, Analyst 133 (11) (2008) 1498–1500, doi:10.1039/b803355b.
[12] Q.S. Li, G.Y.H. Lee, C.N. Ong, C.T. Lim, AFM indentation study of breast cancer cells, Biochem. Biophys. Res. Commun. 374 (2008) 609–613.
[13] Q.S. Li, G.Y.H. Lee, C.N. Ong, C.T. Lim, Probing the elasticity of breast cancer cells using AFM, in: IFMBE Proceedings, Volume 23, 2009, pp. 2122–2125.
[14] E.M. Darling, S. Zauscher, F. Guilak, Viscoelastic properties of zonal articular chondrocytees measured by atomic force microscopy, Osteoarthr. Cartil. 14 (6) (2006) 571–579.
[15] E.M. Darling, M. Topel, S. Zauscher, T. P.Vail, F. Guilak, Viscoelastic properties of human mesenchymally-derived stem cells and primary osteoblasts, chondrocytes, and adipocytes, J. Biomech. 41 (2) (2008) 454–464.
[16] E. Evans, A. Young, Apparent viscosity and cortical tension of blood granulocytes determined by micropipette aspiration, Biophys. J. 56 (1989) 151–160.
[17] C. Dong, R. Skalak, Leukocyte deformability: finite element modeling of large viscoelastic deformation, J. Theor. Biol. 158 (2) (1992) 173–193.
[18] J.L. Drury, M. Dembo, Aspiration of human neutrophils: effects of shear thinning and cortical dissipation, Biophys. J. 81 (6) (2001) 3166–3177.

[19] P. Bursac, G. Lenormand, B. Fabry, M. Oliver, D.A. Weitz, V. Viasnoff, J.P. Butler, J.J. Fredberg, Cytoskeletal remodelling and slow dynamics in the living cell, Nat. Mater. 4 (2005) 557–561.
[20] M. Dao, C.T. Lim, S. Suresh, Mechanics of the human red blood cell deformed by optical tweezers, J. Mech. Phys. Solids 51 (2003) 2259–2280.
[21] M. Radmacher, Studying the mechanics of cellular processes by atomic force microscopy, Cell Mech. 83 (2007) 347–372.
[22] P.A.L. Fernandes, M. delcea, A.G. Skirtach, H. Mohwald, A. Fery, Quantification of release from microcapsules upon mechanical deformation with AFM, Soft Matter 6 (2010) 1879–1883.
[23] H. Hertz, On the contact of elastic solids, J. Reine Angew. Math. 92 (1882) 156–171.
[24] K.B. Bernick, T.P. Prevost, S. Suresh, S. Socrate, Biomechanics of single cortical neurons, Acta Biomater. 7 (3) (2011) 1210–1219.
[25] G.T. Charras, M.A. Horton, Determination of cellular strains by combined atomic force microscopy and finite element modeling, Biophys. J. 83 (2) (2002) 858–879.
[26] H. Ladjal, J.-L. Hanus, A. Pillarisetti, C. Keefer, A. Ferreira, J.P. Desai, Atomic force microscopy-based single-cell indentation: experimentation and finite element simulation, in: Proceedings of IEEE/RSJ International Conference on Intelligent Robots and Systems, 2009, doi:10.1109/IROS.2009.5354351.
[27] N. Nguyen, A. Wineman, A. Waas, Compression of fluid-filled polymeric capsules and inverse analysis to determine nonlinear viscoelastic properties, Int. J. Solids Struct. 62 (2015) 8–17.
[28] J. Sacks, W.J. Welch, T.J. Mitchell, H.P. Wynn, Design and analysis of computer experiments, Stat. Sci. 4 (4) (1989) 409–423.
[29] S.N. Lophaven, H.B. Nielsen, J. Sondergaard, DACE: A Matlab Kriging Toolbox. Technical Report, Technical University of Denmark, 2002.
[30] N.V. Queipo, R.T. Haftka, W. Shyy, T. Goel, R. Vaidyanathan, P.K. Tucker, Surrogate-based analysis and optimization, Prog. Aerosp. Sci. 41 (2005) 1–28.
[31] A. Forrester, A. Sóbester, A. Keane, Engineering Design via Surrogate Modelling: A Practical Guide, John Wiley & Sons, Ltd., 2008.
[32] P.A. Gustafson, A.M. Waas, The influence of adhesive constitutive parameters in cohesive zone finite element models of adhesively bonded joints, Int. J. Solids Struct. 46 (2009) 2201–2215.
[33] C. Heinrich, A.M. Waas, Measuring the in-situ matrix properties in fiber reinforced composites, in: Proceedings of the ASME 2009 International Mechanical Engineering Congress & Exposition, 2009.
[34] Veeco InstrumentsInc., Dimension Icon Instruction Manual-G, Veeco Instruments, Inc., Plainview, NY, USA, 2010.
[35] G.A. Matei, E.J. Thoreson, J.R. Pratt, D.B. Newell, N.A. Burnham, Precision and accuracy of thermal calibration of atomic force microscopy cantilevers, Rev. Sci. Instrum. 77 (8) (2006), doi:10.1063/1.2336115.
[36] D.J. Taatjes, B.T. Mossman, Cell Imaging Techniques: Methods and Protocols, Humana Press, Totowa, NJ, 2005.
[37] S. Moreno-Flores, R. Benitez, Md. Vivanco, J.L. Toca-Herrera, Stress relaxation and creep on living cells with the atomic force microscope: a means to calculate elastic moduli and viscosities of cell components, Nanotechnology 21 (2010) 445101–445108.
[38] R.H.W. Lam, S. Weng, W. Lu, J. Fu, Live-cell subcellular measurement of cell stiffness using a microengineered stretchable micropost array membrane, Integr. Biol. 4 (10) (2012) 1289–1298.
[39] Dassault Systèmes Simulia Corp., ABAQUS-v6.10: ABAQUS User's Manual 6.10, Dassault Systèmes Simulia Corp., Providence, RI, USA, 2010.
[40] R.A. Harouaka, M. Nisic, S.-Y. Zheng, Circulating tumor cell enrichment based on physical properties, J. Lab. Autom. 18 (6) (2013) 455–468.
[41] S. Leporatti, D. Vergara, A. Zacheo, V. Vegaro, G. Maruccio, R. Cingolani, R. Rinaldi, Cytomechanical and topological investigation of MCF-7 cells by scanning force microscopy, Nanotechnology 20 (5) (2009) 055103-1–055103-6.
[42] P.J. Cumpson, P. Zhdan, J. Hedley, Calibration of AFM cantilever stiffness: a microfabricated array of reflective springs, Ultra-microscopy 100 (2004) 241–251.
[43] M.E. Dokukin, N.V. Guz, I. Sokolov, Quantitative study of the elastic modulus of loosely attached cells in AFM indentation experiments, Biophys. J. 104 (10) (2013) 2123–2131.